Alpha and gamma oscillations characterize feedback and feedforward processing in monkey visual cortex

Timo van Kerkoerle[a,1], Matthew W. Self[a], Bruno Dagnino[a], Marie-Alice Gariel-Mathis[a], Jasper Poort[a], Chris van der Togt[a], and Pieter R. Roelfsema[a,b,c,1]

[a]Department of Vision and Cognition, Netherlands Institute for Neurosciences, Royal Netherlands Academy of Arts and Sciences (KNAW), 1105 BA, Amsterdam, The Netherlands; [b]Department of Integrative Neurophysiology, Center for Neurogenomics and Cognitive Research, Vrije Universiteit, 1081HV, Amsterdam, The Netherlands; and [c]Psychiatry Department, Academic Medical Center, 1105 AZ, Amsterdam, The Netherlands

This Feature Article is part of a series identified by the Editorial Board as reporting findings of exceptional significance.

Edited by Terrence J. Sejnowski, Salk Institute for Biological Studies, La Jolla, CA, and approved August 8, 2014 (received for review February 22, 2014)

Cognitive functions rely on the coordinated activity of neurons in many brain regions, but the interactions between cortical areas are not yet well understood. Here we investigated whether low-frequency (α) and high-frequency (γ) oscillations characterize different directions of information flow in monkey visual cortex. We recorded from all layers of the primary visual cortex (V1) and found that γ-waves are initiated in input layer 4 and propagate to the deep and superficial layers of cortex, whereas α-waves propagate in the opposite direction. Simultaneous recordings from V1 and downstream area V4 confirmed that γ- and α-waves propagate in the feedforward and feedback direction, respectively. Microstimulation in V1 elicited γ-oscillations in V4, whereas microstimulation in V4 elicited α-oscillations in V1, thus providing causal evidence for the opposite propagation of these rhythms. Furthermore, blocking NMDA receptors, thought to be involved in feedback processing, suppressed α while boosting γ. These results provide new insights into the relation between brain rhythms and cognition.

neuronal synchronization | attention | perceptual organization | phase coherence | Granger causality

Areas of the visual cortex are arranged hierarchically, with low-level areas representing simple features and higher areas representing the more complex aspects of the visual world (1, 2). Neurons in many visual areas are coactive during the perception of a visual stimulus and it is difficult to disentangle the influences of lower areas onto higher areas from the effects that go in the opposite direction (3). Studies of visual cognition could benefit enormously from markers of cortical activity that distinguish between feedforward and feedback effects. One such putative marker is cortical oscillatory activity, because oscillations of different frequencies have been proposed to propagate either in feedforward or in the feedback direction (4, 5), but experimental evidence for this view is sparse (6).

Low-frequency rhythms, like the α-rhythm—which is particularly pronounced in the visual cortex—have been proposed to characterize spontaneous activity (7, 8) as the α-rhythm increases when the subject closes the eyes (9). More recent observations have also implicated α-oscillations in the active suppression of irrelevant, unattended information (10, 11). In contrast, the high-frequency γ-rhythm increases if visual stimuli are presented, and in particular if they are task-relevant (12, 13). One influential hypothesis has been that γ-oscillations play a role in feature binding (14), but later studies cast doubt on this proposal (15, 16). A more recent hypothesis holds that γ-oscillations facilitate the communication between cortical areas (17), but both evidence in favor of this proposal (18) and against it (19–22) have been presented. Although the causal role of oscillatory rhythms in cognition is therefore not undisputed, it would also be of great value if oscillations could be used as markers for feedforward and feedback effects (23).

We therefore aimed to resolve, to our knowledge for the first time, the laminar pattern of low- and high-frequency oscillations in the primary visual cortex (V1) with a high spatial resolution during a texture-segregation task that requires interactions between visually driven activity and top-down influences from higher areas. For comparison, we also examined oscillatory coupling between V1 and extrastriate area V4 in the same task. Moreover, herein we used two new causal approaches to test directionality. First, we applied microstimulation in one area while recording the oscillations in the other area. Second, we locally infused blockers of AMPA and NMDA receptors thought to be differentially involved in feedforward and feedback processing (24, 25). All our results converged onto a straightforward conclusion: γ-oscillations in the visual cortex travel in the feedforward direction, whereas α-oscillations index feedback effects.

Results

We first investigated the power and the timing of oscillatory activity in the different layers of area V1. Anatomical studies demonstrated that the feedforward input from the lateral geniculate nucleus (LGN) arrives predominantly in layer 4C with a weaker input into layer 6 (26), whereas feedback connections from higher visual areas target layers 1, 2, and 5, avoiding layer 4 (27, 28). If α and γ activity travel in opposite directions through the cortex, this might therefore be visible in the laminar profile of these rhythms in V1.

To measure oscillatory activity in V1, we recorded multiunit neuronal activity (MUA) and local field potentials (LFP) using

Significance

One of the main unresolved questions in cognitive neuroscience is how low-level and high-level areas of the visual cortex interact with each other during perception and cognition. We investigated whether cortical oscillations can be used to distinguish feedforward from feedback processing. We studied the propagation of α- and γ-oscillations through the cortical layers and between different visual cortical areas. We induced oscillations in different areas with microstimulation and influenced them using a pharmacological approach. The results of these experiments demonstrate that γ-oscillations propagate in the feedforward direction, whereas α-oscillations propagate in the feedback direction. We conclude that high- and low-frequency oscillations provide markers of feedforward and feedback processing, respectively.

Author contributions: T.v.K. and P.R.R. designed research; T.v.K., M.W.S., B.D., M.-A.G.-M., and J.P. performed research; T.v.K. and C.v.d.T. contributed new analytic tools; T.v.K. analyzed data; and T.v.K. and P.R.R. wrote the paper.

The authors declare no conflict of interest.

This article is a PNAS Direct Submission.

Freely available online through the PNAS open access option.

See Commentary on page 14316.

[1]To whom correspondence may be addressed. Email: p.roelfsema@nin.knaw.nl or t.van.kerkoerle@nin.knaw.nl.

This article contains supporting information online at www.pnas.org/lookup/suppl/doi:10.1073/pnas.1402773111/-/DCSupplemental.

laminar electrodes that span the cortical depth with contact points spaced 100-μm apart (Fig. 1 *A* and *B*). An important advantage of these laminar electrodes is that they permit the computation of the current-source density (CSD), which estimates currents flowing into and out of neurons in different layers (29, 30). We determined the cortical depth of the laminar electrode in each recording session with the CSD response triggered by the appearance of a checkerboard stimulus (31). The stimulus evoked a characteristic CSD profile with a current sink in layer 4C and a current source in the deep layers (*SI Appendix*, Fig. S1). These sinks and sources coincided with the onset of the visual response in the MUA.

Oscillatory Activity in V1 in a Texture-Segregation Task. We trained monkeys to carry out a figure-ground segregation task in which they detected an orientation-defined figure (Fig. 1 *C* and *D*) (32). The monkeys started a trial by directing their gaze to a fixation point and, after a delay of 300 ms, a full screen texture appeared with texture elements, with one orientation and a square figure (4° size) of the opposite orientation (Fig. 1*C*). After an additional 300 ms of fixation, the monkey made an eye movement toward the figure to obtain a juice reward. On each trial, the figure appeared at one of three locations at the same eccentricity. In one of these conditions, the neurons' receptive fields (RFs) fell on the figure center; in the other two conditions the RFs fell on the background (Fig. 1*D*). We balanced the orientation of the line elements across trials so that the texture elements inside the RFs were on average identical across conditions, and we ensured that the RFs of none of the recording sites overlapped with the figure edge. As previously reported (32), MUA in V1 (24 penetrations with a total of $n = 493$ recording sites, 13 penetrations in monkey S and 11 penetrations in monkey E) was stronger if the neurons' RF fell on the figure than when it fell on the background (Fig. 2*A*), a modulatory effect that most likely depends on feedback from higher areas (33–35).

Examination of the LFP also revealed a prominent signature of figure-ground organization. The background texture evoked a strong low frequency oscillation, which could be seen in single trials (arrows in Fig. 2*B*), but the low-frequency oscillations elicited by the figure were weaker. To further characterize these oscillations, we computed the power spectrum in a window from 150 to 350 ms from stimulus onset. This analysis revealed a prominent peak in the lower frequencies (5–15 Hz), which was larger if the RF fell on the background than if it fell on the figure (Fig. 2*C* and *SI Appendix*, Fig. S2 *A* and *D*) and also stronger than in the prestimulus period (Fig. 2*C* and *SI Appendix*, Fig. S2*C*) (*t* test, $n = 493$, $P < 0.001$ for both comparisons). We next analyzed of the LFP–MUA coherence, focusing on the internally generated oscillations by first subtracting the evoked potential (*SI Appendix*, Fig. S3), and found that the MUA was also more strongly locked to the low-frequency rhythm if the RF fell on the

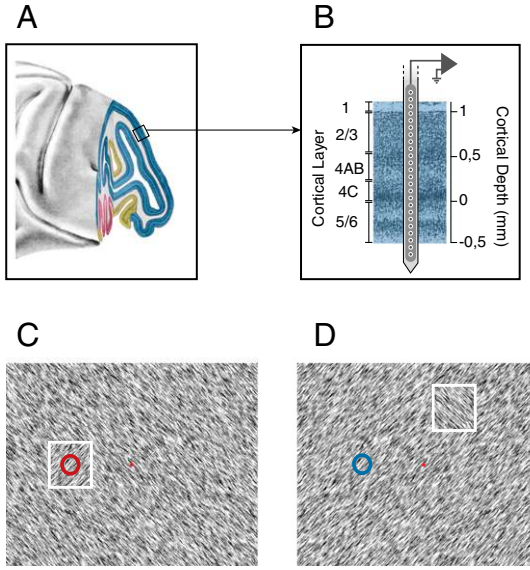

Fig. 1. Laminar recordings. (*A*) Lateral view of the macaque brain. Blue region corresponds to area V1. (*B*) Laminar recording with the multisite linear electrode (Plexon Inc. U-probe). (*C* and *D*) Texture segregation stimulus with a figure of one orientation placed on a background with the orthogonal orientation. The neurons' receptive field (circle) fell on the figure (white square, not visible to the monkey) (*C*) or on the background (*D*).

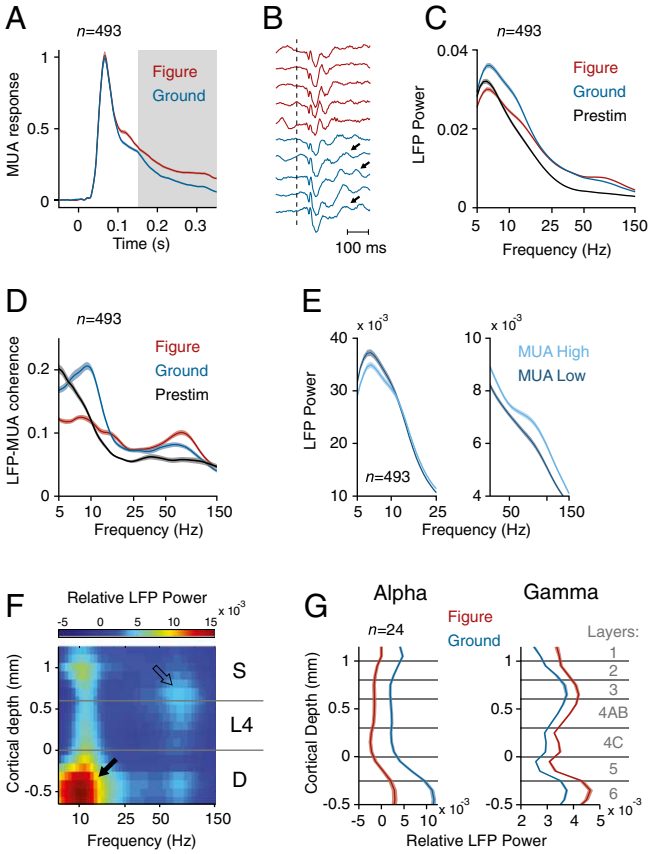

Fig. 2. Neuronal activity in the texture-segregation task. (*A*) Average MUA response in V1 evoked by the figure (red trace) and the background (blue trace) ($n = 493$ recording sites). Gray area highlights the modulation period (150–350 ms after stimulus onset). (*B*) Example LFP responses in successive trials at an example electrode, elicited by image elements of the figure (red) and background (blue). Dotted line indicates the stimulus onset, arrows indicate slow frequency oscillations. (*C*) Average LFP power spectrum (arbitrary units) evoked by the figure (red trace) and background (blue trace) during the modulation period and the prestimulus period (200–0 ms before stimulus onset) (black trace). (*D*) Average LFP–MUA coherence in the figure (red trace) and background condition (blue trace) during the modulation period, and the prestimulus period (black trace). The dashed lines indicate the LFP–MUA coherence for shuffled trials. (*E*) LFP power spectra calculated for the 50% trials with lowest (dark blue lines) and highest MUA response (light blue lines) in the conditions with the RF on the background. (*F*) Laminar profile of the increase in LFP power evoked by the background (power is shown in pseudocolor, arbitrary units, log scale). Black arrow, α-activity in the deep layers. Open arrow, γ-activity in upper layer 4 and the superficial layers. (*G*) Laminar profile of LFP power in the α- (5–15 Hz) and γ-band (40–90 Hz) in the conditions with the RF on the figure (red traces) and background (blue traces). Shaded areas show SEM in all plots ($n = 493$ recording sites), when they are difficult to see the SEM is small.

background (Fig. 2*D* and *SI Appendix*, Fig. S2*F*). The spectral resolution for the low frequencies was limited by the short duration of the computational window (200 ms), but we obtained a comparable results when we analyzed trials with longer reaction times so that we could use a longer time window of 300 ms (*SI Appendix*, Fig. S4). We also analyzed catch trials with a homogeneous background where the monkeys were required to maintain gaze on the fixation point for 700 ms (*SI Appendix*, Fig. S5 *A–C*). The MUA in these catch trials was similar to when the figure was placed outside the neurons' RF (*SI Appendix*, Fig. S5*H*). The LFP power spectrum and the LFP–MUA coherence in the catch trials were similar to that in the background condition (time-window of 550 ms; spectral resolution of ∼1.8 Hz) with a peak at ∼10 Hz, indicative of an α-oscillation (*SI Appendix*, Fig. S5 *F* and *G*). The α-peak also remained in a later time-window (400–700 ms after stimulus onset) (*SI Appendix*, Fig. S5*I*), confirming that the α-oscillation did not depend on the initial stimulus-evoked activity. The increase of the α-rhythm when the RF fell on the background compared with when it fell on the figure and compared with the prestimulus period is in line with previous reports that α indexes the suppression of irrelevant information (10, 11). Moreover, we found that trials with more LFP α-power (5–15 Hz) had a weaker MUA response (Fig. 2*E*) (corrected coefficient = −0.05, *t* test, $n = 493$, $P < 0.05$) (36) in further support of this idea.

In contrast to the low-frequency rhythm, the γ-rhythm was stronger in the figure representation than in the background. This increase in γ was visible in the LFP power spectrum (Fig. 2*C* and *SI Appendix*, Fig. S2 *A* and *E*) and also in the coherence between the MUA and the LFP (Fig. 2*D* and *SI Appendix*, Fig. S2*G*) (*t* test, $n = 493$, $P < 0.001$ for both comparisons). When we sorted trials according to γ-power (40–90 Hz), trials with a higher γ were associated with a stronger MUA response (Fig. 2*E*) (corrected coefficient = 0.3, *t* test, $P < 0.001$) (37). We also investigated the intermediate β-band (15–30 Hz), but β-power and coherence were only weakly modulated by the task (Fig. 2 *C* and *D* and *SI Appendix*, Fig. S2*A*). The weak β-oscillations differentiate V1 from the primary somatosensory cortex, where β-power is much more prominent (38).

To analyze the profile of LFP power across the layers, we divided them into four compartments: layers 1/2, layer 3, layer 4, and layers 5/6. The α-power was strongest in layers 5/6 (*t* test, $n =$ 24 penetrations, all $Ps < 0.001$) with a secondary peak in layer 1/2 (layers 1/2 higher than layers 3 and 4; *t* test, $P < 0.001$) (Fig. 2 *F* and *G*) as has been observed previously (13, 39). In contrast, γ-power was stronger in layer 3 than in the other layers (Fig. 2 *F* and *G*) (*t*-test, all $Ps < 0.001$) (39, 40). The laminar pattern of LFP power was similar, irrespective of whether the RF fell on figure or ground (Fig. 2*G*). Thus, the cortical mechanisms that generate the α- and γ-rhythm appear to be similar for the figure and background, but task-relevance modulates the amplitude of these rhythms.

Propagation of α- and γ-Oscillations Through the Layers of V1. The use of a laminar electrode with a fine spacing between contact points provided us with a unique opportunity to investigate the propagation of rhythmic activity from one layer to the next. We investigated the LFP in all layers, aligning activity to the LFP troughs in layer 4C (*SI Appendix*, Fig. S6). To detect the time of α-troughs we filtered the LFP between 8 and 12 Hz and registered the times of the minima. These narrow filter settings were only used to detect trough times; all further analyses were performed with the broad-band LFP signal (*SI Appendix*, Fig. S6*D*).

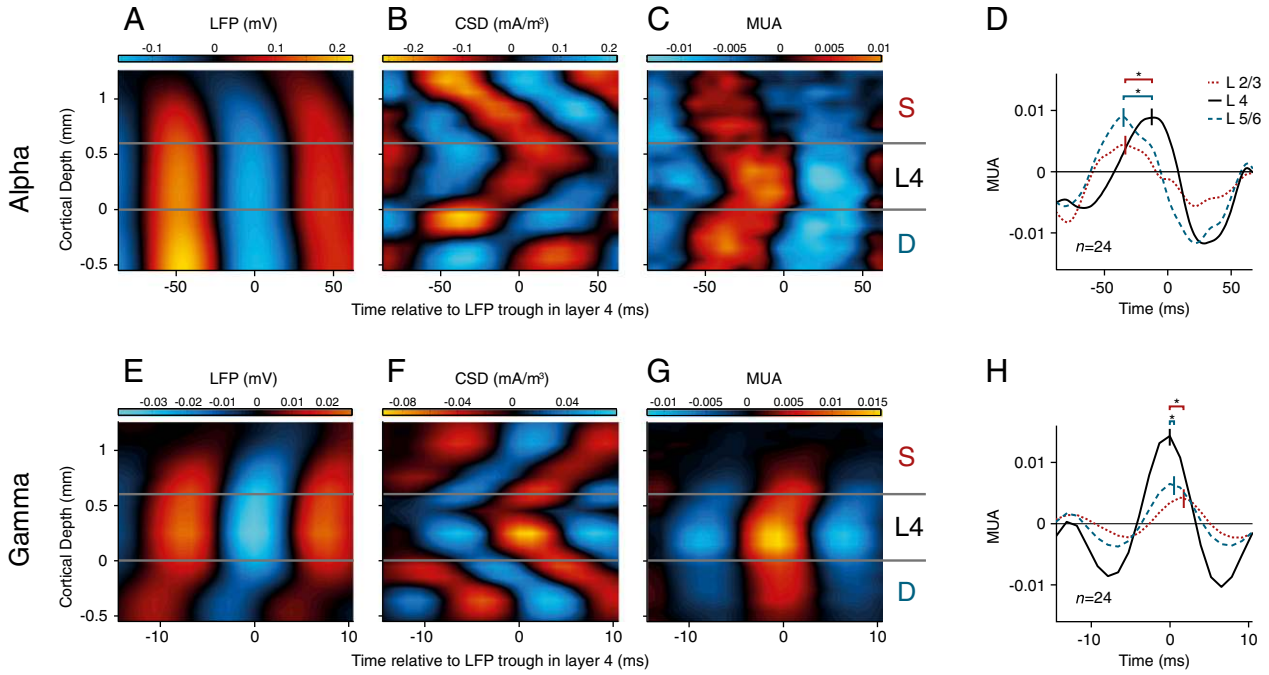

Fig. 3. Laminar profile of cortical oscillations. To determine the average laminar profile of the LFP, CSD, and MUA relative to the α- and γ-oscillations, we aligned the data to the troughs of the LFP in layer 4. (*A*) Laminar profile of the LFP (mV) relative to the α-troughs in a window from 150 to 300 ms after stimulus onset, averaged across 24 penetrations. The LFP was relatively homogeneous across the layers. Negative potentials are shown in blue, positive potentials in red. (*B*) Average laminar profile of the CSD (mA/m^3) relative to LFP troughs in layer 4 for the α-rhythm. Current sinks are shown in red, sources in blue. (*C*) MUA aligned to the LFP troughs in layer 4. Red colors show MUA that is higher than the average and blue colors show that MUA lower than the average. The MUA was normalized to the visually driven activity 150–300 ms after stimulus onset. The scale therefore denotes the fraction of the visually driven MUA response that synchronized to the LFP troughs in layer 4 in the 8- to 12-Hz frequency range. (*D*) Average MUA ($n = 24$ penetrations) in layer 2/3 (red dotted curve), 4 (black continuous curve), and 5/6 (blue dashed curve) relative to the trough of the α-wave in layer 4. *Significant difference in phase (*t* test, $P < 0.005$). (*E–H*) Same analysis as in *A–D*, but now the data were aligned to the troughs of the γ-rhythm (55–65 Hz) in layer 4.

We used the α-trough time-points to compute the average trough-aligned LFP, in the same way that one would align the LFP to the stimulus presentations to compute the evoked potential. We applied this analysis to the broad-band LFP in the background condition where α was most pronounced and averaged across all penetrations ($n = 24$). In the LFP, the α-oscillations were relatively coherent across cortical depth (Fig. 3*A*), but this signal also contains contributions from volume conduction. The CSD provides a local measure for the sinks and sources underlying the LFP in the different layers. The CSD profile had the shape of a chevron, with a succession of sinks starting in feedback recipient layers 1, 2, and 5 that propagated toward layer 4 during the α-cycle (Fig. 3*B*). The MUA was also coupled to the LFP troughs (Fig. 3*C*), as predicted by the significant coherence between these signals in the α-range (Fig. 2*D*). Interestingly, we also observed phase differences between MUA in different cortical layers. The earliest MUA coincided with the current sinks in layers 1, 2, and 5 (Fig. 3*C*). MUA in layer 4 lagged MUA in the deep and superficial layers by 12 and 10 ms, respectively (Fig. 3*D*) (*t* test, $n = 24$ penetrations, both comparisons $P < 0.005$). When we repeated this analysis for other frequency bands, we found that MUA in superficial and deep layers preceded MUA in layer 4 for all frequencies between 5 and 15 Hz (*SI Appendix*, Fig. S7). The same laminar profile was found before stimulus onset, indicating that it was general feature of α-oscillations, which did not depend on the presence of a visual stimulus (*SI Appendix*, Fig. S8).

The phase lags in the MUA were less pronounced than in the CSD (Fig. 3 *B* and *C*), smaller phase differences that might be explained by the neurons' extended dendritic trees. Neurons sample synaptic input from multiple layers so that the timing of somatic spikes across layers might become more similar than the timing of synaptic inputs in different layers. For example, some layer 4 cells receive input trough their dendrites in layer 2/3 so that they can start to fire action potentials before the α-related synaptic input arrives in layer 4. To directly investigate the phase relationship between spikes and synaptic input, we analyzed the coherence between the MUA and the layer-specific CSD for the α-frequencies (Fig. 4*A*). In this analysis, we averaged MUA across layers, but we obtained qualitatively comparable results if we separately analyzed MUA from the superficial layers, layer 4, or deep layers (*SI Appendix*, Fig. S9). We found four coherence peaks, in layers 1/2, 4, 5, and 6. The phase analysis for the α-rhythm revealed that MUA was in phase with sinks in layers 1/2 and 5 [mean phase advance of CSD sink relative to MUA in L1/2, $23 \pm 6°$ (SEM); L5, $-2 \pm 8°$; $n = 24$] but with sources in layers 4 and 6 (mean phase in L4, $-174 \pm 7°$; L6, $171 \pm 5°$). These results suggest

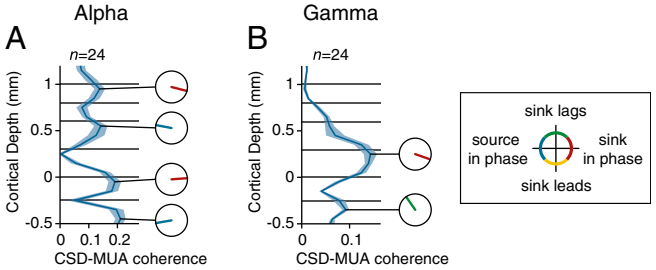

Fig. 4. Laminar profile of CSD–MUA coherence and phase. (*A*) Laminar profile of coherence between the layer-specific CSD and the MUA averaged across all layers for the α-band (RF on the background). There were four peaks in the coherence and the small circles show the phase of the CSD relative to the MUA. Red colors indicate that MUA was in phase with a sink in layers 1/2 and 5. Blue colors indicate that the MUA was in phase with a source. (*B*) Laminar profile of the CSD–MUA coherence in the γ-frequency range. Note that the MUA was in phase with a sink in layer 4.

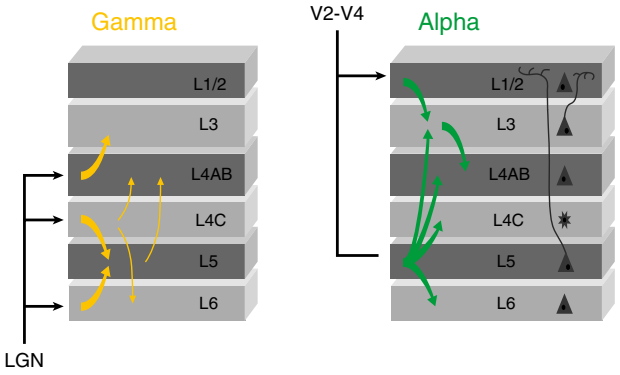

Fig. 5. Schematic representation of Granger causality between layers for the γ- (*Left*) and α-band (*Right*). Thick arrows indicate Granger causality stronger than 0.015, thin arrows for the γ-band indicate Granger causality between 0.005 and 0.015 (not shown for the α-band to prevent crowding).

that the spikes locking to the α-rhythm are driven by sinks in layers 1/2 and 5, which are the main targets of feedback connections.

We next analyzed the propagation of activity during γ-oscillations. We detected troughs by filtering the LFP between 55 and 65 Hz and then used these time-points to analyze the broad-band LFP, CSD, and the MUA (*SI Appendix*, Fig. S6). Strikingly, γ-oscillations exhibited the opposite sequence of sinks across the layers (Fig. 3 *E–G*). The γ-cycle started with a sink in layer 4, the recipient of feedforward input, and the sinks then propagated to the superficial and deep layers. Spiking activity in layer 4 coincided with the layer 4 current sink, and was delayed by 1 ms in the deep layers (*t* test, $n = 24$, $P < 0.05$) and by 2 ms in the superficial layers ($P < 0.005$) (Fig. 3*H*) (41), a phase delay that occurred for all frequencies between 20 and 100 Hz (*SI Appendix*, Fig. S7). The analysis of γ-coherence between MUA and CSD revealed two peaks. The first coherence peak reflected the coincidence of the MUA with a current sink in layer 4 [mean phase advance of CSD sink relative to MUA: $17 \pm 4°$ (SEM); $n = 24$] and the second coherence peak occurred in layer 6, where a current sink lagged the MUA by $116 \pm 5°$ (Fig. 4*B*). These results suggest that the γ-cycle starts with excitatory input into layer 4, the main target of feedforward connections from the LGN.

The propagation of α- and γ-oscillations through the layers was highly consistent between monkeys (*SI Appendix*, Fig. S10). Interestingly, it was also relatively invariant across conditions with the RF on the background (Fig. 3), the figure (*SI Appendix*, Fig. S11 *A–F*), and catch trials (*SI Appendix*, Fig. S11 *G–L*). We observed a comparable invariance in the phase relation between CSD and MUA, which did not depend strongly on the presence of a figure in the RF (compare Fig. 4 with *SI Appendix*, Fig. S12). Thus, figure-ground segregation influences the amplitude of the oscillations, but the cortical mechanisms that generate these rhythms appear to be invariant.

We replicated these results with a phase coherency analysis that does not depend on the detection of troughs. We analyzed the phase of the CSD and MUA in the different layers relative to the LFP in layer 4. For the γ-oscillations, the phase of the CSD and MUA in layer 4 was earlier than that in the other layers (*SI Appendix*, Fig. S13) (*t* test, $n = 24$, $P < 0.001$ for both MUA and CSD), in accordance with the feedforward laminar profile. α-Oscillatory activity showed the opposite profile with a phase advance of the deep and superficial layers relative to layer 4 (*SI Appendix*, Fig. S13) ($P < 0.001$ for both MUA and CSD). Thus, the opposite propagation of α- and γ-oscillations through the cortical layers is a robust finding that does not depend on details of the analysis method.

We complemented the analysis of phase differences by measuring Granger causality between the CSDs in the different layers. If oscillations are propagated between layers, then activity in one layer should forecast activity in the next better than the other way around, implying a significant directionality in the Granger causal interactions (38). As a first step in this analysis, we calculated the average coherence of CSDs between sites on the laminar probe with a distance of 200 μm, and found peaks at 10 and 80 Hz (*SI Appendix*, Fig. S14), in accordance with the LFP–MUA coherence (Fig. 2*D*). The Granger causality analysis also revealed a peak around 10 Hz, in accordance with a previous study (42), and a broader peak in the γ-range (*SI Appendix*, Fig. S15). Fig. 5 summarizes the Granger–causal interactions between layers with a significant directionality in the α- and γ-range. It can be seen that Granger causality in the α-range was directed from the superficial and deep layers toward layer 4, in accordance with the analysis of phase differences (Fig. 3*B*). The Granger causality showed a strong directionality from layer 5 to layers 6, 4C, 4AB, and 3 (permutation test, $P < 0.001$), from layer 1/2 to layer 3 (permutation test, $P < 0.001$), and from layer 3 to layer 4AB (permutation test, $P < 0.001$), indicating that the α-rhythm originates from the feedback recipient layers in V1. The Granger causality in the γ-range (30–90 Hz) showed a strong directionality from layer 4AB to layer 3, from layers 4C to layer 5 and 6, and from layer 6 to layer 5 (permutation test, all *Ps* < 0.001) (Fig. 5 and *SI Appendix*, Fig. S15), in line with the trough-triggering analysis (Fig. 3), implying that the γ-rhythm originates from the V1 layers that receive feedforward input from the LGN.

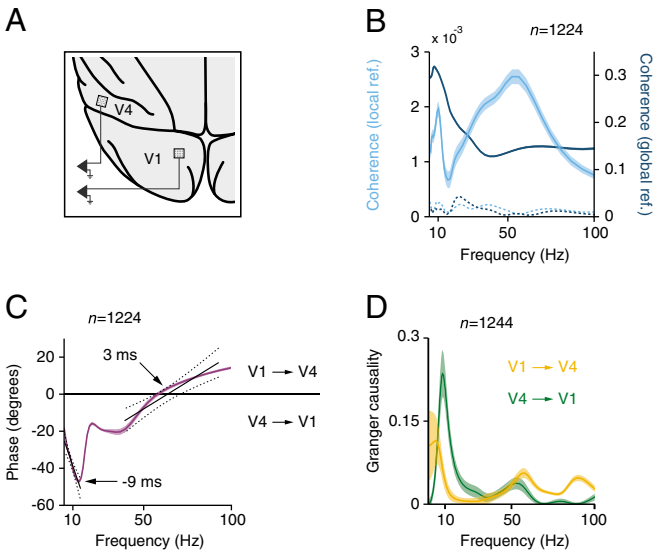

Fig. 7. Array recordings in areas V1 and V4. (*A*) Schematic representation of implanted electrode arrays in V1 and V4 with overlapping RF's. (*B*) Coherence between the LFP in V1 and V4 in a window from 150 to 350 ms after stimulus onset when the neurons' receptive fields fell on the background. Shaded areas show SEM (n = 1,224 pairs). The cyan curve shows the coherence between the locally referenced LFP in the two areas (y axis scale shown left). Blue curve, coherence between LFP signals referenced to a low-impedance epidural electrode (y axis scale on the right). Dotted lines indicate the V1–V4 coherence for shuffled trials. (*C*) Phase relationship between LFP in V1 and V4. Black lines show least-square linear fits to the phase of α and γ as function of frequency. Dashed lines indicate 95% confidence intervals ($P < 0.001$). (*D*) Average Granger causality of the LFP from V1 to V4 (yellow line) and from V4 to V1 recording sites (green line). Shaded areas show SEM (n = 1,224 pairs).

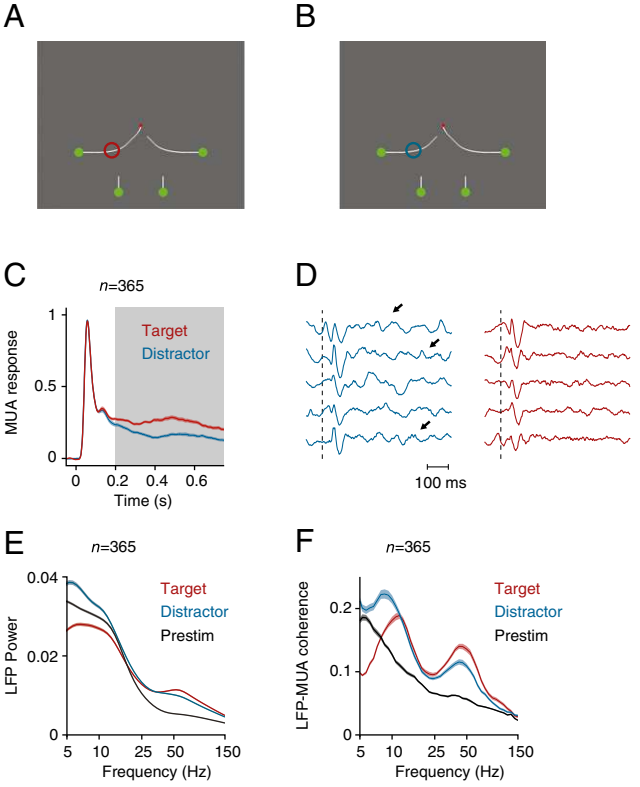

Fig. 6. Curve-tracing task where the monkey had to mentally trace the target curve that was connected to the fixation point. (*A* and *B*) We placed either the target curve (*A*, red circle) or one of the distractor curves in the RF (*B*, blue circle). (*C*) Neuronal activity averaged across all V1 recording sites in two monkeys evoked by the target (red trace) and the distractor curve (blue trace). Gray area highlights the time window for spectral analysis (200–750 ms after stimulus onset). (*D*) Example LFP responses in successive single trials elicited by the target (red) and distractor curve (blue). Dotted line indicates the stimulus onset, arrows point to low frequency oscillations. (*E*) LFP power spectrum elicited by the target and distractor curve and during prestimulus period (200–0 ms before stimulus onset) (black trace). (*F*) LFP–MUA coherence evoked by the target and distractor curve during the epoch of response modulation (200–750 ms after stimulus onset) and during the prestimulus period (black trace). Shaded areas show SEM in all plots (n = 365 recording sites), when they are difficult to see the SEM is small.

Curve-Tracing Task. Texture-defined figures are intrinsically salient and induce stimulus-driven attention shifts (43). We therefore investigated if these results generalize to another task where the attention shifts depend on familiarity with the task. Two monkeys mentally traced a target curve, which was connected to a red fixation point, while ignoring three distractor curves (Fig. 6 *A* and *B*). We showed previously that subjects solve this task by directing attention to the target curve and by ignoring the distractors (44, 45). The monkeys viewed the stimulus for 750 ms, and we ensured that the contour element in the neurons' RF was the same across conditions so that we could directly investigate the influence of attention shifts on neuronal activity in V1 (eight penetrations in monkey R and eight penetrations in monkey E, with a total of n = 365 recording sites). As in previous work (e.g., ref. 46), the attended curve evoked a stronger MUA response than the distractor curves (Fig. 6*C*) ($P <$ 0.001, sign-test). Also in this task, the ignored curve elicited a low-frequency oscillation that was visible in individual trials (Fig. 6*D*), and we could now examine LFP power and LFP–MUA coherence in a longer time window (from 200 to 750 ms after stimulus onset) (Fig. 6 *E* and *F*). Our results replicated those in the texture-segregation (compare with Fig. 2). The distractor curve evoked a significant increase in low frequency power ($P <$ 0.001, sign-test), whereas the target curve elicited stronger power in the γ-frequency range ($P < 0.001$, sign-test). The LFP–MUA

coherence revealed that MUA was locked to these rhythms (Fig. 6*F*) and demonstrated that the center frequency of the low-frequency oscillation was 10 Hz. Moreover, the propagation of neuronal activity through the cortical layers was comparable to that in the texture-segregation task (*SI Appendix*, Fig. S16), implying that these results generalized across tasks.

Coupling Between V1 and V4. We found that γ-waves start in input layer 4, whereas α-waves start in feedback recipient layers 1, 2, and 5. Is this opposite progression of oscillations through the cortical layers associated with corresponding time-lags between lower and higher visual areas? Previous studies in cats and using EEG recordings in humans suggested a phase lead of lower areas over higher areas for γ-oscillations and a phase lag for α-oscillations (6, 47, 48). To investigate the synchrony between areas of the monkey visual cortex in the texture-segregation task, we simultaneously recorded the LFP in V1 and downstream area V4 with chronically implanted microelectrode arrays, with an electrode length of 1 or 1.5 mm, in two other monkeys (n = 34 recording sites in V1, n = 36 recording sites in V4, 7 recording sessions) (Fig. 7*A*). The V1 and V4 RFs overlapped (*SI Appendix*, Fig. S17). We first examined the coherence between the LFPs in the two areas in the background condition and observed that it was significant for both the α- and the γ-range compared with a shuffle control (t test, n = 1,224 pairs, $P < 0.001$) (Fig. 7*B*). For the coherence and power analysis, we referenced the LFP to another electrode within the same array (interelectrode distance of 0.4 mm). The interareal coherence was much lower than in a recent study using epidural EEG recording above V1 and V4 (49) (interelectrode distance of 2–3 mm), as predicted by previous work (50). Indeed, the coherence between the V1 and V4 LFP referenced to a low impedance epidural electrode was two orders-of-magnitude higher (blue in Fig. 6*B*), but coherence computed in this way may also contain the contribution of sources that are picked up by the common reference. We next examined the phase relation (epidural reference) and observed a phase-lead of area V4 for the lower frequencies (Fig. 7*C*), which increased with frequencies between 5 and 12 Hz. This finding is consistent with a relatively fixed time delay between V4 and V1 that translates into larger phase lags at higher frequencies. The slope of the phase relation provides an estimate of this delay for the α-band, which was ∼9 ms (limitations of this method have been pointed out by ref. 51). The slope inverted above 15 Hz, and the V1 phase lag changed into a phase lead in the γ-band. Although less linear, the slope of this phase relation in the γ-range suggested that V1 led V4 by ∼3 ms. We used Granger causality (global reference) to further investigate the directionality of the coupling between V1 and V4 (Fig. 7*D*). We observed a narrow peak around 10 Hz directed in the feedback direction, from V4 to V1 (permutation test, $P < 0.01$). In contrast, Granger causality in the γ-range was stronger in the feedforward direction, from V1 to V4 (permutation test $P < 0.01$), in accordance with the analysis of phase delays (Fig. 7*C*). Thus, the interareal coupling during figure-ground segregation supports the hypothesis that γ- and α-rhythms index feedforward and feedback processing, respectively.

Microstimulation in V1 and V4. We next tested this hypothesis with a causal approach by combining electrical microstimulation in one area with the recording of LFP in the other area, in two monkeys (six and eight recording sessions with stimulation in V1 and V4, respectively). We again used the chronically implanted microarrays with overlapping RFs, but we now stimulated one area and recorded neuronal activity in the other one. We applied microstimulation in V1 for 20 ms (five pulses at 200 Hz; amplitude 50–100 μA), starting 150 ms after the onset of the texture segregation stimulus. Microstimulation had a negligible effect on the monkeys' accuracy (above 98%), which was expected because the task was not designed to provide sensitive measures of the

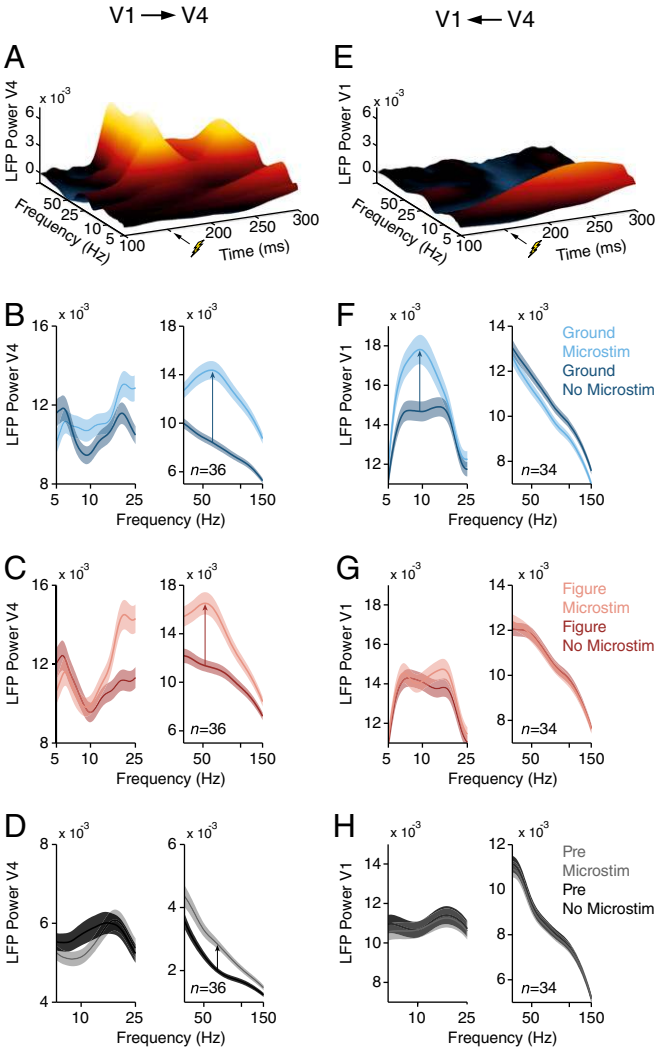

Fig. 8. Effects of microstimulation in areas V1 and V4. (*A*) Effect of microstimulation of V1 on the LFP power spectrum in V4. Stimulation (five pulses, 200 Hz) was applied in the conditions with the RF on the background from 150 to 170 ms after stimulus onset in the texture segregation task. The power in each time bin represents the center of a time window (Morlet wavelet) with a length equal to one cycle of the corresponding frequency. (*B* and *C*) Power spectrum in V4 with (lighter curve) and without V1 microstimulation (darker curve) if the RF fell on the background (*B*) or figure (*C*). The analysis window was from 0 to 200 ms (50–100 ms) after microstimulation for α (γ). Shaded areas show SEM (n = 36 recording sites). (*D*) Influence of V1 microstimulation from 150 to 130 ms before stimulus onset on V4 power. (*E*) Effect of V4 microstimulation on the power spectrum in V1 in the background condition (n = 34 recording sites). (*F–H*) Power spectrum in V1 with (lighter curves) and without V4 microstimulation (darker curves) if the RFs fell on the background (*F*), figure (*G*), or in the prestimulus epoch (*H*).

monkeys' performance. It induced γ-oscillations in V4 (t test, n = 36 V4 recording sites, $P < 0.001$, 200–250 ms after stimulus onset, both in the figure and background condition) but had little effect on V4 α-power ($P > 0.3$, 150–350 ms after stimulus onset) (Fig. 8 *A–C*). The effect of V1 microstimulation did not strongly depend on whether the neurons' RF fell on the background (Fig. 8*B*) or figure (Fig. 8*C*). Moreover, a similar effect occurred if microstimulation occurred in the fixation epoch, 150 ms before the texture was presented (t test, n = 36, $P < 0.001$ for γ; $P > 0.25$ for α) (Fig. 8*D*). Thus, the effect of V1 microstimulation on V4 power did not depend strongly on the visual stimulus, which is in accordance with a driving effect of the feedforward connections.

We also carried out the opposite experiment, microstimulating in V4 while recording in V1. If the neurons' RF fell on the background, V4 microstimulation with the same timing (amplitude 30–60 μA) caused an increase in the V1 α-rhythm (t test, $n = 34$ V1 recording sites, $P < 0.001$, 150–350 ms after stimulus onset), but it suppressed the γ-rhythm ($P < 0.05$, 200–250 ms after stimulus onset) (Fig. 8 *E* and *F*). The effect of V4 microstimulation on V1 was stimulus-dependent. If the figure fell in the neurons' RFs, it blocked the increase in α elicited by V4 microstimulation as well as the decrease in gamma (Fig. 8*G*). Interestingly, V4 microstimulation also had little effect on V1 power in the fixation epoch, when the monkeys were looking at a blank screen (t test, $n = 34$, $P > 0.5$ for α and γ, 150–0 ms before stimulus onset) (Fig. 8*H*). Thus, V1 neurons are particularly susceptible for the V4 feedback effects when their RFs fall on the background. Furthermore, these microstimulation results, taken together, provide causal evidence that γ-oscillations travel in the feedforward direction, whereas α-waves travel in the feedback direction.

Pharmacological Intervention in V1. We used pharmacology as an additional causal method to probe the directionality of α- and γ-oscillations. Theoretical studies proposed that the feedforward drive of a cortical neuron depends on AMPA-receptors, whereas feedback effects depend more on NMDA-receptors (24). A recent neurophysiological study using the texture-segregation task demonstrated that AMPA-blockers indeed reduce the visually driven response, whereas NMDA-blockers decrease the difference in activity evoked by the figure and background (25), which depends on feedback connections (33, 35). If α-oscillations signify feedback processing, then α-power might decrease if NMDA-receptors are blocked. We used laminar probes with a fluid line for local pressure injection of small quantities (<80 nL) of pharmacological substances in V1 while the monkeys carried out the texture-segregation task (*SI Appendix*, Fig. S18*A*). We first measured the effective diffusion distance of our injections with CNQX (an AMPA-receptor blocker), which reliably reduces neural responses. CNQX injections reduced neural activity over a distance of ∼1.5 mm (*SI Appendix*, Fig. S18*B*).

To block NMDA-receptors, we applied the broad-spectrum NMDA-antagonists APV (8 penetrations in two monkeys) and ifenprodil, which blocks NMDA-receptors with the NR2B subunit (11 penetrations in two monkeys). The small drug injections generally did not interfere with the monkeys' accuracy, which was higher than 97%, but they did have a profound influence on the power spectrum of the LFP. Both NDMA-receptor blockers suppressed the α-frequencies of the LFP and enhanced the γ-frequencies (Fig. 9). These effects occurred if the neurons' RF fell on the background (Fig. 9 *A* and *B*) (t test, APV $n = 156$ sites, ifenprodil $n = 200$, both drugs $P < 0.001$ for α; $P < 0.05$ for APV and $P < 0.001$ for ifenprodil for γ) and also if it fell on the figure (Fig. 9 *D* and *E*) (both drugs $P < 0.001$ for α; $P < 0.05$ for APV and $P < 0.001$ for ifenprodil for γ). The two NMDA-blockers have opposing effects on visually driven activity (25), which implies that their influence on α- and γ-oscillations are not caused by changes in neuronal excitability. In the control experiments where we blocked the AMPA-receptors with CNQX ($n = 113$ sites in seven penetrations in two monkeys), we observed a reduction in the LFP power across all frequencies (Fig. 9 *C* and *F*) (t test, $n = 113$, $P < 0.001$ for α and γ in either stimulus condition), as is expected for a drug that causes a general decrease of cortical activity. Thus, NMDA-receptor activity is important for the α-rhythm, which fits with the relatively long time constant of these receptors (52) and is in accordance with their role in feedback processing (24, 25).

Discussion

Our results provide four convergent lines of evidence that the γ-rhythm is a signature of feedforward processing, whereas the α-rhythm indexes feedback effects. First, our results demonstrate, to our knowledge for the first time, that γ-waves start in layer 4, the input layer of cortex, and are then propagated to the superficial and deep layers. α-Waves are initiated in layers 1, 2, and 5, the targets of corticocortical feedback connections in V1 (27) and propagate in the opposite direction, toward layer 4. Second, simultaneous recordings in V1 and V4 showed that the γ-rhythm propagates from V1 to V4, whereas the α-rhythm propagates in the opposite direction. Third, electrical microstimulation provided the first causal evidence that feedforward processing induces γ-oscillations in a higher visual area and that feedback causes α-activity in a lower area. Fourth, we found that local application of blockers of the NMDA-receptor, which is important for feedback effects (25), suppressed α-oscillations and enhanced γ-oscillations. Taken together, these results provide strong evidence for the opposite directionality of α- and γ-oscillations.

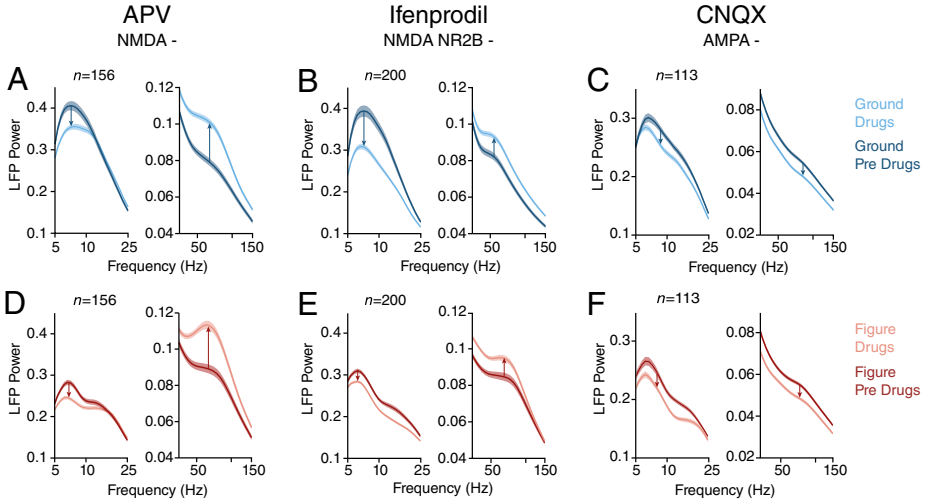

Fig. 9. Effects of glutamate-receptor antagonists in V1. (*A*) Effect of the NMDA-receptor blocker APV on the LFP power spectrum ($n = 156$ sites), in a window from 150 to 350 ms after stimulus onset with the RF on the background. Blue trace, predrug epoch; cyan trace, after drug application. (*B*) Effect of ifenprodil, another blocker of the NMDA-receptor ($n = 200$). (*C*) Effect of the AMPA-receptor blocker CNQX ($n = 113$). (*D–F*) Same as *A–C* but for the condition with the RF on the figure. Shaded areas show SEM.

Figure-ground organization mainly influenced the amplitude of the oscillations but their laminar patterns remained the same, and we obtained similar results with shifts of attention in the curve-tracing task. Thus, task-relevance influences the amplitude of the rhythms, but the cortical mechanisms that generate them appear to be task and stimulus invariant.

Mechanisms Underlying the α-Rhythm. Our analysis of the coherence between MUA and the CSD during α-oscillations revealed that spikes coincide with sinks in feedback recipient layers 1/2 and 5 (27, 28) and with sources in layers 4 and 6 (26) (Fig. 4). This finding is of considerable interest because layer 5 cells, thought to be involved in the generation of α (53, 54), are particularly sensitive to coincident input to their basal and apical dendritic trees (55, 56) and their apical dendrites have a resonance in the 5- to 10-Hz frequency range (5, 57). α-Coherence between spikes and the CSD was also measured by Bollimunta et al. (42) but the present study is, to our knowledge, the first to resolve the laminar pattern with a high resolution because of a denser spacing of contact points on the electrodes.

The sinks that started in layers 1/2 and 5 propagated toward input layer 4 during the α-cycle. We obtained a similar result for MUA, which also started in the superficial and deep layers and was delayed in layer 4 during the α-cycle. The propagation of activity toward layer 4 could rely on the input it receives from layers 5/6 (58-61) and 2/3 (60). The results therefore support the hypothesis that α is a signature of feedback effects.

Mechanisms Underlying the γ-Rhythm. Our data revealed that spiking activity during the γ-cycle coincided with a sink in layer 4C, which was followed by a succession of sinks propagating toward the superficial and deep layers. Moreover, layer 4 MUA locking to the γ-rhythm preceded MUA in superficial and deep layers, in line with a previous study in squirrel monkey (41). These results suggest that the γ-oscillation in V1 is elicited by thalamic input, which is in accordance with the finding that trials with a stronger MUA response also elicited more γ. In combination with in vitro studies demonstrating that γ-oscillations are of cortical origin (5), our results suggest that the thalamic input enables a cortical loop that generates these high-frequency rhythms.

Our laminar recordings thereby provided new mechanistic insight into generation of cortical rhythms. The opposite directionalities of γ- and α-oscillations represent a strong constraint for cortical circuit models that aim to explain the generation of these rhythms.

Directionality Between V1 and V4. The simultaneous V1–V4 recordings demonstrated that the opposite directionalities of the α- and γ-rhythms coexist for a single combination of visual cortical areas within a single task. The relationship between the frequency and phase-delay in the two areas suggested that V1 leads V4 by 3 ms for the γ-rhythm but lags V4 by 9 ms for α. This difference between time-lags may seem surprising because feedforward and feedback connections have similar conduction times (62), but our pharmacological results suggest that it may be explained by a difference in synaptic integration. The time constant of NMDA channels, which play a role in the feedback effects, is longer than that of AMPA channels that are important for the feedforward propagation of activity to higher visual areas (25).

Our analysis of phase shifts and Granger causality between V1 and V4 confirmed the propagation of α-waves in the feedback direction, in accordance with some (48, 63) but not all (64) previous EEG-recordings in humans. At first sight, this result appears to contradict a recent finding that Granger causality between V1 and V2 in the α-range is strongest in the feedforward direction (18). We suspect that methodological differences (the previous study only selected electrode combinations with high γ-coherence) and perhaps differences between tasks are responsible for this discrepancy.

The feedforward signature of γ is in line with recent studies showing stronger Granger causality for γ from V1 to V2 and from V1 to V4 than in the opposite direction (18, 49, 65). It is also reminiscent of a study in cats, showing that γ-oscillations propagate from the LGN to V1 with an average delay of ∼2 ms (47).

A modeling study by Vierling-Claassen et al. (66) suggested that pyramidal cells interact with fast-spiking interneurons to generate γ-oscillations, whereas they interact with low-threshold spiking interneurons to generate the α-rhythm. In this context, our findings raise the possibility that feedforward connections preferentially influence the putative loop that involves fast-spiking cells, whereas feedback connections target low-threshold spiking interneurons, a hypothesis that could be explored in future work (e.g., by recording from genetically identified single neurons during α- and γ-oscillations in mice).

Causal Tests of Directionality. To our knowledge, our electrical microstimulation experiments provide the first causal evidence that feedforward processing induces γ-oscillations in a higher visual area and that feedback causes α-activity in a lower area. We used electrode arrays for microstimulation, positioned 1 or 1.5 mm below the cortical surface; they were presumably in layers 4 or 5, but the effects of microstimulation on neuronal activity are relatively homogeneous across cortical depth (67, 68). Microstimulation activates axons in the vicinity of the electrode tip (68, 69) and can cause orthodromic and antidromic stimulation effects in another area. Antidromic effects occur if axon terminals of projection neurons are stimulated and action potentials travel back to their cell-bodies in another area. Orthodromic effects occur either by the direct or by transsynaptic activation of projection neurons with cell bodies in the area that is stimulated. At the current levels used by us, most neurons are stimulated transsynaptically (68). Accordingly, previous studies demonstrated that orthodromic stimulation effects are many times stronger than antidromic effects even between areas with strong direct projections (62, 70, 71). The direct connectivity between V1 and V4 is relatively sparse (72), and the antidromic contribution to our findings was therefore presumably even smaller than in these previous studies.

V4 microstimulation only caused an increase in V1 α if the neurons' RF fell on the background (Fig. 8). This finding is important for two reasons. First, antidromic stimulation effects should be invariant across visual stimulation conditions. The stimulus dependence of V4 microstimulation effects therefore confirms the predominance of orthodromic, transsynaptic stimulation effects. Second, the finding that V4 stimulation only induced α in V1 if the neurons' RFs fell on the background suggests that α-oscillations are signature of suppressive feedback effects. This suggestion is supported by our finding that trials with strong α were associated with a weak MUA response, as well as preliminary results that V4 microstimulation reduces firing rates of V1-neurons in the texture-segregation task (73). The influence of V4 stimulation on the V1 α-rhythm could be generated by the cortico-cortical feedback connections, but our results do not exclude the possibility that these effects are mediated in part through the thalamus (74). Specifically, connections from the pulvinar also target the superficial layers of V1 and may provide a source of top-down influences (75–77). We used V1 microstimulation to probe the feedforward effects and found that it elicited γ-power in area V4 without a strong influence on the V4 α-rhythm. Interestingly, this increase in γ was relatively independent of the visual stimulus in the neurons' RF, in accordance with a driving influence of the feedforward connections, and indeed, our preliminary results revealed that V1 microstimulation increases V4 spiking activity (73).

Our second causal experiment influenced the activity of glutamate receptors with a pharmacological approach. Theoretical work (24) implicated NMDA-receptor activity in cortico-cortical feedback effects. A recent study (25) confirmed this prediction by demonstrating that figure-ground modulation in V1, which depends on feedback (35), indeed requires NMDA-receptor activity, whereas visually driven activity in V1 primarily depends on AMPA-receptors. Thus, NMDA-blockers reduce feedback influences, and our finding that they reduce α-oscillations is in line with the hypothesis that α-oscillations signify feedback effects. This finding is also in accordance with previous results in cortical slices where NMDA blockers suppress the lower frequencies (53). At the same time, we found that NMDA-receptor blockers enhanced γ-oscillations, in accordance with previous results obtained with the systemic application of NMDA antagonists in rodents (78) and with local application in the visual cortex of monkeys (79).

The Influence of Perceptual Organization on the α- and γ-Rhythm. The finding that the γ- and α-rhythms signal feedforward and feedback processing is neutral with respect to their putative role in information processing. Many studies have reported that selective attention enhances the γ-rhythm (12, 13, 49, 80). The increased γ may be instrumental in the propagation of sensory information toward higher areas (17), but it could also be a side-effect of a more efficient feedforward information flow for attended stimuli. Earlier studies reported that the presentation of a visual stimulus suppresses the α-rhythm (8, 80–82). Our laminar recordings only revealed α suppression at the representation of the figure and only in the middle and superficial layers (Fig. 2*G*), in line with recent studies (13, 83). The selective enhancement of the α-rhythm in the background of the texture stimulus and its association with weaker neuronal activity suggests that it reflects the active suppression of irrelevant information (10, 11, 84). Such a suppressive feedback effect is in accordance with a role of corticocortical feedback in surround suppression (85–87) and inhibitory effects of selective attention in early visual areas (88, 89). A previous model of the interactions between cortical areas for texture segregation proposed that the orientation of the image elements that are part of the figure is registered in higher visual areas, which feedback to suppress V1 responses to background elements with the orthogonal orientation and disinhibit activity evoked by figural image elements with the same orientation (90). The putative disinhibitory top-down feedback influence on the figure representation is in line with the low α-power with the figure in the neuron's RF. Our results do not exclude that feedback, in addition to its putative disinhibitory effect, also has direct excitatory effects to enhance the neuronal representation of relevant image elements (91, 92). Such an excitatory feedback signal might be weaker, or not show up in a spectral analysis if it targets different synapses that do not cause synchronized activity. Our experiments with the curve-tracing task and a comparison with previous work (12, 13, 49, 80) indicate that the effects of task-relevance of α- and γ-power generalize across tasks.

Irrespective of the precise functional significance of these brain rhythms, our results demonstrate that α- and γ-oscillations characterize feedback and feedforward processing in the visual cortex. This new insight can now be exploited to gain a deeper understanding of the role of feedforward and feedback influences in visual cognition.

Experimental Procedures

Six adult macaque monkeys (S, E, R, B, J, and C) were trained to do a texture-segregation task. A texture stimulus was presented 300 ms after the monkey directed gaze to a fixation period. The stimulus was a whole-screen texture with one orientation with a figural region of 4 × 4° with the orthogonal orientation (Fig. 1 *D* and *E*). After another fixation epoch of 300 ms, the monkey received a reward for making a saccade to the texture-defined figure. The figure could appear at three possible locations, with the location of the figure rotated by 120°. The texture stimuli were constructed so that on average, precisely the same contour elements were present inside the RF across the different conditions (details in *SI Appendix*).

In monkeys S, E, and R extracellular recordings in V1 were performed with multicontact "U" probes (Plexon) with 24 contact points spaced 100-μm apart. A fluid line allowed the application of pharmacological substances by pressure injection with a Hamilton syringes (1 μL). The depth of the probe was determined by measuring the CSD evoked by a full-screen 100% contrast checkerboard. We estimated the location of the border between layer 5 and layer 4C as the polarity reversal from current sinks in layer 4C to current sources in the deep layers (*SI Appendix*, Fig. S1).

In monkeys B, J, and C we obtained extracellular recordings in V1 and V4 using grids of 4 × 5 microelectrodes (Cyberkinetics Neurotechnology Systems). For the power and coherence analysis we locally referenced the LFP to an electrode within the same array. For the electrical microstimulation experiments, we delivered trains of five biphasic pulses of 500-μs duration at a frequency of 200 Hz with an amplitude in the range of 30–100 μA. The anode and cathode electrode were on the same array, reducing the stimulation artifact in the other area where we recorded LFPs. Statistical significance was assessed using paired Student *t* tests. See *SI Appendix* for further information about the paradigm, neuronal recordings and data analysis.

ACKNOWLEDGMENTS. We thank Kor Brandsma, Dave Vleesenbeek, and Anneke Ditewig for biotechnical assistance; Pascal Fries, Tobias H. Donner, and Charles E. Schroeder for helpful comments on the manuscript; and Guido Cilissen for help with the design of Fig. 1*A*. The work was supported by a Netherlands Organization for Scientific Research-Vici grant, and the European Union Seventh Framework Program (Project 269921 "BrainScaleS") and European Research Council Grant Agreement 339490 (to P.R.R.).

1. Zeki SM (1978) Functional specialisation in the visual cortex of the rhesus monkey. *Nature* 274(5670):423–428.
2. Felleman DJ, Van Essen DC (1991) Distributed hierarchical processing in the primate cerebral cortex. *Cereb Cortex* 1(1):1–47.
3. Lamme VAF, Roelfsema PR (2000) The distinct modes of vision offered by feedforward and recurrent processing. *Trends Neurosci* 23(11):571–579.
4. Engel AK, Fries P, Singer W (2001) Dynamic predictions: Oscillations and synchrony in top-down processing. *Nat Rev Neurosci* 2(10):704–716.
5. Wang XJ (2010) Neurophysiological and computational principles of cortical rhythms in cognition. *Physiol Rev* 90(3):1195–1268.
6. von Stein A, Chiang C, König P (2000) Top-down processing mediated by interareal synchronization. *Proc Natl Acad Sci USA* 97(26):14748–14753.
7. Adrian E (1944) Brain rhythms. *Nature* 153(3882):360–362.
8. Yu J, Ferster D (2010) Membrane potential synchrony in primary visual cortex during sensory stimulation. *Neuron* 68(6):1187–1201.
9. Berger H (1929) Über das elektroenkephalogramm des menschen. *Arch Psychiatr Nervenkr* 87(1):527–570.
10. Klimesch W, Sauseng P, Hanslmayr S (2007) EEG alpha oscillations: The inhibition-timing hypothesis. *Brain Res Brain Res Rev* 53(1):63–88.
11. Jensen O, Mazaheri A (2010) Shaping functional architecture by oscillatory alpha activity: Gating by inhibition. *Front Hum Neurosci* 4:186.
12. Fries P, Reynolds JH, Rorie AE, Desimone R (2001) Modulation of oscillatory neuronal synchronization by selective visual attention. *Science* 291(5508):1560–1563.
13. Buffalo EA, Fries P, Landman R, Buschman TJ, Desimone R (2011) Laminar differences in gamma and alpha coherence in the ventral stream. *Proc Natl Acad Sci USA* 108(27):11262–11267.
14. Singer W, Gray CM (1995) Visual feature integration and the temporal correlation hypothesis. *Annu Rev Neurosci* 18:555–586.
15. Thiele A, Stoner G (2003) Neuronal synchrony does not correlate with motion coherence in cortical area MT. *Nature* 421(6921):366–370.
16. Roelfsema PR, Lamme VAF, Spekreijse H (2004) Synchrony and covariation of firing rates in the primary visual cortex during contour grouping. *Nat Neurosci* 7(9):982–991.
17. Fries P (2009) Neuronal gamma-band synchronization as a fundamental process in cortical computation. *Annu Rev Neurosci* 32:209–224.
18. Roberts MJ, et al. (2013) Robust gamma coherence between macaque V1 and V2 by dynamic frequency matching. *Neuron* 78(3):523–536.
19. Chalk M, et al. (2010) Attention reduces stimulus-driven gamma frequency oscillations and spike field coherence in V1. *Neuron* 66(1):114–125.
20. Lima B, Singer W, Chen NH, Neuenschwander S (2010) Synchronization dynamics in response to plaid stimuli in monkey V1. *Cereb Cortex* 20(7):1556–1573.
21. Ray S, Maunsell JH (2010) Differences in gamma frequencies across visual cortex restrict their possible use in computation. *Neuron* 67(5):885–896.
22. Jia X, Smith MA, Kohn A (2011) Stimulus selectivity and spatial coherence of gamma components of the local field potential. *J Neurosci* 31(25):9390–9403.
23. Siegel M, Donner TH, Engel AK (2012) Spectral fingerprints of large-scale neuronal interactions. *Nat Rev Neurosci* 13(2):121–134.

24. Dehaene S, Changeux JP (2011) Experimental and theoretical approaches to conscious processing. *Neuron* 70(2):200–227.
25. Self MW, Kooijmans RN, Supèr H, Lamme VA, Roelfsema PR (2012) Different glutamate receptors convey feedforward and recurrent processing in macaque V1. *Proc Natl Acad Sci USA* 109(27):11031–11036.
26. Lund JS (1988) Anatomical organization of macaque monkey striate visual cortex. *Annu Rev Neurosci* 11:253–288.
27. Rockland KS, Virga A (1989) Terminal arbors of individual "feedback" axons projecting from area V2 to V1 in the macaque monkey: A study using immunohistochemistry of anterogradely transported *Phaseolus vulgaris*-leucoagglutinin. *J Comp Neurol* 285(1):54–72.
28. Anderson JC, Martin KA (2009) The synaptic connections between cortical areas V1 and V2 in macaque monkey. *J Neurosci* 29(36):11283–11293.
29. Mitzdorf U (1985) Current source-density method and application in cat cerebral cortex: Investigation of evoked potentials and EEG phenomena. *Physiol Rev* 65(1):37–100.
30. Buzsáki G, Anastassiou CA, Koch C (2012) The origin of extracellular fields and currents—EEG, ECoG, LFP and spikes. *Nat Rev Neurosci* 13(6):407–420.
31. Schroeder CE, Tenke CE, Givre SJ, Arezzo JC, Vaughan HG, Jr (1991) Striate cortical contribution to the surface-recorded pattern-reversal VEP in the alert monkey. *Vision Res* 31(7-8):1143–1157.
32. Lamme VAF (1995) The neurophysiology of figure-ground segregation in primary visual cortex. *J Neurosci* 15(2):1605–1615.
33. Lamme VAF, Supèr H, Spekreijse H (1998) Feedforward, horizontal, and feedback processing in the visual cortex. *Curr Opin Neurobiol* 8(4):529–535.
34. Hupé JM, et al. (1998) Cortical feedback improves discrimination between figure and background by V1, V2 and V3 neurons. *Nature* 394(6695):784–787.
35. Poort J, et al. (2012) The role of attention in figure-ground segregation in areas V1 and V4 of the visual cortex. *Neuron* 75(1):143–156.
36. Haegens S, Nácher V, Luna R, Romo R, Jensen O (2011) α-Oscillations in the monkey sensorimotor network influence discrimination performance by rhythmical inhibition of neuronal spiking. *Proc Natl Acad Sci USA* 108(48):19377–19382.
37. Ray S, Maunsell JH (2011) Different origins of gamma rhythm and high-gamma activity in macaque visual cortex. *PLoS Biol* 9(4):e1000610.
38. Brovelli A, et al. (2004) Beta oscillations in a large-scale sensorimotor cortical network: Directional influences revealed by Granger causality. *Proc Natl Acad Sci USA* 101(26):9849–9854.
39. Maier A, Adams GK, Aura C, Leopold DA (2010) Distinct superficial and deep laminar domains of activity in the visual cortex during rest and stimulation. *Front Syst Neurosci* 4:4.
40. Xing D, Yeh CI, Burns S, Shapley RM (2012) Laminar analysis of visually evoked activity in the primary visual cortex. *Proc Natl Acad Sci USA* 109(34):13871–13876.
41. Livingstone MS (1996) Oscillatory firing and interneuronal correlations in squirrel monkey striate cortex. *J Neurophysiol* 75(6):2467–2485.
42. Bollimunta A, Mo J, Schroeder CE, Ding M (2011) Neuronal mechanisms and attentional modulation of corticothalamic α oscillations. *J Neurosci* 31(13):4935–4943.
43. Roelfsema PR, Tolboom M, Khayat PS (2007) Different processing phases for features, figures, and selective attention in the primary visual cortex. *Neuron* 56(5):785–792.
44. Scholte HS, Spekreijse H, Roelfsema PR (2001) The spatial profile of visual attention in mental curve tracing. *Vision Res* 41(20):2569–2580.
45. Houtkamp R, Spekreijse H, Roelfsema PR (2003) A gradual spread of attention during mental curve tracing. *Percept Psychophys* 65(7):1136–1144.
46. Roelfsema PR, Lamme VAF, Spekreijse H (1998) Object-based attention in the primary visual cortex of the macaque monkey. *Nature* 395(6700):376–381.
47. Castelo-Branco M, Neuenschwander S, Singer W (1998) Synchronization of visual responses between the cortex, lateral geniculate nucleus, and retina in the anesthetized cat. *J Neurosci* 18(16):6395–6410.
48. Ito J, Nikolaev AR, van Leeuwen C (2005) Spatial and temporal structure of phase synchronization of spontaneous alpha EEG activity. *Biol Cybern* 92(1):54–60.
49. Bosman CA, et al. (2012) Attentional stimulus selection through selective synchronization between monkey visual areas. *Neuron* 75(5):875–888.
50. Bullock TH, McClune MC (1989) Lateral coherence of the electrocorticogram: A new measure of brain synchrony. *Electroencephalogr Clin Neurophysiol* 73(6):479–498.
51. Lindemann M, Raethjen J, Timmer J, Deuschl G, Pfister G (2001) Delay estimation for cortico-peripheral relations. *J Neurosci Methods* 111(2):127–139.
52. Traynelis SF, et al. (2010) Glutamate receptor ion channels: Structure, regulation, and function. *Pharmacol Rev* 62(3):405–496.
53. Silva LR, Amitai Y, Connors BW (1991) Intrinsic oscillations of neocortex generated by layer 5 pyramidal neurons. *Science* 251(4992):432–435.
54. Roopun AK, et al. (2008) Period concatenation underlies interactions between gamma and beta rhythms in neocortex. *Front Cell Neurosci* 2:1.
55. Larkum ME, Zhu JJ, Sakmann B (1999) A new cellular mechanism for coupling inputs arriving at different cortical layers. *Nature* 398(6725):338–341.
56. Larkum M (2013) A cellular mechanism for cortical associations: An organizing principle for the cerebral cortex. *Trends Neurosci* 36(3):141–151.
57. Ulrich D (2002) Dendritic resonance in rat neocortical pyramidal cells. *J Neurophysiol* 87(6):2753–2759.
58. Gilbert CD, Wiesel TN (1979) Morphology and intracortical projections of functionally characterised neurones in the cat visual cortex. *Nature* 280(5718):120–125.
59. Fitzpatrick D, Lund JS, Blasdel GG (1985) Intrinsic connections of macaque striate cortex: Afferent and efferent connections of lamina 4C. *J Neurosci* 5(12):3329–3349.
60. Binzegger T, Douglas RJ, Martin KA (2004) A quantitative map of the circuit of cat primary visual cortex. *J Neurosci* 24(39):8441–8453.
61. Thomson AM (2010) Neocortical layer 6, a review. *Front Neuroanat* 4:13.
62. Girard P, Hupé J-M, Bullier J (2001) Feedforward and feedback connections between areas V1 and V2 of the monkey have similar rapid conduction velocities. *J Neurophysiol* 85(3):1328–1331.
63. Patten TM, Rennie CJ, Robinson PA, Gong P (2012) Human cortical traveling waves: Dynamical properties and correlations with responses. *PLoS ONE* 7(6):e38392.
64. Bahramisharif A, et al. (2013) Propagating neocortical gamma bursts are coordinated by traveling alpha waves. *J Neurosci* 33(48):18849–18854.
65. Bastos AM, et al. (2014) Visual areas exert feedforward and feedback influences through distinct frequency channels. Available at http://biorxiv.org/content/early/2014/05/06/004804. Accessed May 21, 2014.
66. Vierling-Claassen D, Cardin JA, Moore CI, Jones SR (2010) Computational modeling of distinct neocortical oscillations driven by cell-type selective optogenetic drive: Separable resonant circuits controlled by low-threshold spiking and fast-spiking interneurons. *Front Hum Neurosci* 4:198.
67. Contreras D, Dürmüller N, Steriade M (1997) Absence of a prevalent laminar distribution of IPSPs in association cortical neurons of cat. *J Neurophysiol* 78(5):2742–2753.
68. Butovas S, Schwarz C (2003) Spatiotemporal effects of microstimulation in rat neocortex: A parametric study using multielectrode recordings. *J Neurophysiol* 90(5):3024–3039.
69. Histed MH, Bonin V, Reid RC (2009) Direct activation of sparse, distributed populations of cortical neurons by electrical microstimulation. *Neuron* 63(4):508–522.
70. Bullier J, McCourt ME, Henry GH (1988) Physiological studies on the feedback connection to the striate cortex from cortical areas 18 and 19 of the cat. *Exp Brain Res* 70(1):90–98.
71. Movshon JA, Newsome WT (1996) Visual response properties of striate cortical neurons projecting to area MT in macaque monkeys. *J Neurosci* 16(23):7733–7741.
72. Markov NT, et al. (2011) Weight consistency specifies regularities of macaque cortical networks. *Cereb Cortex* 21(6):1254–1272.
73. Dagnino B, Gariel MA, Roelfsema PR (2013) Feedforward and feedback propagation of electrically induced activity in the visual cortex. *SfN Abstracts* (Society for Neuroscience, San Diego), no. 638.08.
74. Lopes da Silva FH, Vos JE, Mooibroek J, Van Rotterdam A (1980) Relative contributions of intracortical and thalamo-cortical processes in the generation of alpha rhythms, revealed by partial coherence analysis. *Electroencephalogr Clin Neurophysiol* 50(5-6):449–456.
75. Benevento LA, Rezak M (1975) Extrageniculate projections to layers VI and I of striate cortex (area 17) in the rhesus monkey (*Macaca mulatta*). *Brain Res* 96(1):51–55.
76. Ogren MP, Hendrickson AE (1977) The distribution of pulvinar terminals in visual areas 17 and 18 of the monkey. *Brain Res* 137(2):343–350.
77. Saalmann YB, Pinsk MA, Wang L, Li X, Kastner S (2012) The pulvinar regulates information transmission between cortical areas based on attention demands. *Science* 337(6095):753–756.
78. Hakami T, et al. (2009) NMDA receptor hypofunction leads to generalized and persistent aberrant gamma oscillations independent of hyperlocomotion and the state of consciousness. *PLoS ONE* 4(8):e6755.
79. Herrero JL, Gieselmann MA, Sanayei M, Thiele A (2013) Attention-induced variance and noise correlation reduction in macaque V1 is mediated by NMDA receptors. *Neuron* 78(4):729–739.
80. Fries P, Womelsdorf T, Oostenveld R, Desimone R (2008) The effects of visual stimulation and selective visual attention on rhythmic neuronal synchronization in macaque area V4. *J Neurosci* 28(18):4823–4835.
81. Gray CM, Singer W (1989) Stimulus-specific neuronal oscillations in orientation columns of cat visual cortex. *Proc Natl Acad Sci USA* 86(5):1698–1702.
82. Hipp JF, Engel AK, Siegel M (2011) Oscillatory synchronization in large-scale cortical networks predicts perception. *Neuron* 69(2):387–396.
83. Sejnowski TJ, Paulsen O (2006) Network oscillations: Emerging computational principles. *J Neurosci* 26(6):1673–1676.
84. Bonnefond M, Jensen O (2012) Alpha oscillations serve to protect working memory maintenance against anticipated distracters. *Curr Biol* 22(20):1969–1974.
85. Shushruth S, et al. (2012) Strong recurrent networks compute the orientation tuning of surround modulation in the primate primary visual cortex. *J Neurosci* 32(1):308–321.
86. Gilad A, Meirovithz E, Slovin H (2013) Population responses to contour integration: Early encoding of discrete elements and late perceptual grouping. *Neuron* 78(2):389–402.
87. Nassi JJ, Lomber SG, Born RT (2013) Corticocortical feedback contributes to surround suppression in V1 of the alert primate. *J Neurosci* 33(19):8504–8517.
88. Chen Y, et al. (2008) Task difficulty modulates the activity of specific neuronal populations in primary visual cortex. *Nat Neurosci* 11(8):974–982.
89. Niebergall R, Khayat PS, Treue S, Martinez-Trujillo JC (2011) Multifocal attention filters targets from distracters within and beyond primate MT neurons' receptive field boundaries. *Neuron* 72(6):1067–1079.
90. Roelfsema PR, Lamme VAF, Spekreijse H, Bosch H (2002) Figure-ground segregation in a recurrent network architecture. *J Cogn Neurosci* 14(4):525–537.
91. Shao Z, Burkhalter A (1996) Different balance of excitation and inhibition in forward and feedback circuits of rat visual cortex. *J Neurosci* 16(22):7353–7365.
92. Moore T, Armstrong KM (2003) Selective gating of visual signals by microstimulation of frontal cortex. *Nature* 421(6921):370–373.